Interannual and Decadal Variations of Planetary-Wave Activity, Stratospheric Cooling, and Northern-Hemisphere Annular Mode

Yongyun Hu and Ka Kit Tung

Department of Applied Mathematics

University of Washington

P.O. Box 352420

Seattle, WA 98195-2420

Accepted by *Journal of Climate*, Nov., 2001

Short title: PLANETARY WAVE, ARCTIC OSCILLATION, AND STRATOSPHERIC COOLING

Abstract.

Using 51-year NCEP/NCAR reanalysis data, we study the interannual and decadal variations of planetary-wave activity and its relation to stratospheric cooling, and the Northern-Hemisphere Annular mode (NAM). We find that on interannual timescales winter stratospheric polar temperature is highly correlated on a year-to-year basis with the Eliassen-Palm wave flux from the troposphere, implying a dynamical control of the former by the latter, as often suggested. On timescales of decades, however, the trend in the temperature is not correlated with the trend in planetary-wave activity. In fact, we find that both planetary-wave amplitude and Eliassen-palm flux show little evidence of statistically significant decrease in the past 51 years, while the stratosphere is experiencing a cooling trend and the NAM index has a positive trend during the past 30 years. This suggests that the trends in the winter polar temperature and the NAM index can reasonably be attributed to the radiative cooling of the stratosphere, due possibly to increasing greenhouse gases and ozone depletion. We further show that the positive trend of the NAM index in the past few decades is not through the inhibition of upward planetary wave propagation from the troposphere to the stratosphere, as previously suggested.

1. Introduction

There has been some evidence indicating that the stratosphere has been steadily cooling during the past few decades (Randel and Wu, 1999). Observations show that the Arctic polar vortex has become colder and stronger (Labitzke and Naujokat, 2000), that it persists longer (Newman et al., 1997; Waugh et al., 1999), and that there have been fewer major sudden warmings (There were only two major warmings from 1990 to 2000 (1990/91 and 1998/99) (Labitzke and Naujokat, 2000)). The strengthening of the polar vortex is consistent with the trend of the Northern Annular Mode (NAM) toward the high index phase since 1968 (Thompson and Wallace, 1998).

It is well established that the temperature in the winter polar region of the stratosphere is determined by the balance of two factors: radiative cooling and adiabatic, dynamical heating (Andrews, Holton, and Leovy, 1987). The latter is caused by downwelling in the stratospheric polar region, induced by global-scale wave-driven meridional circulation and thus depends on planetary-wave activity generated in the troposphere. It is such dynamical heating that is responsible for forcing winter polar temperatures above the radiative equilibrium temperature during polar night. Fusco and Salby (1999) and Salby et al. (2000) found that on interannual timescales stratospheric ozone and temperature in the Arctic polar region in winter is regulated by the upward Eliassen-Palm (E-P) flux across the tropopause, and that the two have a strong correlation. A natural question is: Is the long-term stratospheric cooling caused by a long-term decrease of planetary-wave activity in the stratosphere?

Based on their climate model simulations of the doubling CO_2 scenario, Rind et al. (1998), Shindell et al. (1998), and Shindell et al. (1999) speculated that the planetary-wave activity from the troposphere to the stratosphere might have declined due to the increasing greenhouse gases in the atmosphere. They proposed an interesting, plausible feedback mechanism responsible for a decrease of planetary-wave activity in the stratosphere: Both

increasing greenhouse gases in the atmosphere and ozone depletion in the stratosphere would enhance the meridional temperature gradient in the extratropical upper troposphere, with warming in the tropics and cooling in high latitudes. Such an enhanced meridional temperature gradient can lead to a stronger vertical shear of the zonal mean wind, which presumably impedes upward propagation of planetary waves from the troposphere into the stratosphere. In an earlier work, Chen and Robinson (1992) also found in their linear model simulations that vertical wind shear near the tropopause is critical for controlling the passage of planetary waves from the troposphere to the stratosphere. They showed that a weaker vertical wind shear tends to enhance upward planetary-wave propagation across the tropopause. (As we will discuss later, the two groups actually dealt with wind shears at different levels and thus formed very different conclusions.) However, it has not been demonstrated that the effect due to changes of vertical wind shear works in the real atmosphere in the manner suggested.

Recent studies on the so-called Arctic Oscillation (AO) or NAM provide another view on the possible relationship between planetary-wave activity and the stratospheric cooling. A recent survey linking NAM, planetary-wave activity, greenhouse effects, and climate change can be found in Hartmann et al.(2000), which emphasized that NAM may be an internal mode of natural variability of the atmosphere. This internal mode is characterized by its deeply vertically coherent structure extending from the surface to the stratosphere, irregular oscillation on broad timescales, and positive trend toward the high index phase since 1968 (Thompson and Wallace, 1998; Thompson et al., 2000; Wallace, 2000). Using observational data and general circulation model (GCM) output, Limpasuvan and Hartmann (1999, 2000) found that the NAM oscillation between high and low index phases is a result of the internal coupling between the zonal flow and planetary waves. They showed that when data are composited according to high and low NAM indices, at the tropopause level planetary waves are refracted away from the Arctic polar region in the high

index phase, whereas planetary waves are more readily focused into the polar waveguide in the low index phase, where they decelerate the polar jet. This result on the relationship between NAM index phases and planetary-wave behavior concerns only the interannual variation of the NAM index. It is not known whether the long-term positive trend in the NAM index is governed by a mechanism similar to that for the high NAM index phases.

Our purpose in the present paper is twofold. First, we inquire whether planetary-wave activity from the troposphere into the stratosphere has changed systematically in the recent few decades as suggested above. Second, we are concerned with the relationship between wave-driven dynamical heating and the long-term stratospheric cooling trend. We focus attention on the trends of January-mean temperature in Arctic polar region and of the wave-driven dynamical heating during preceding months (November-December-January, NDJ). Section 2 provides the source of the data used in this study. In section 3, we analyze the long-term linear trend in planetary-wave (wavenumber 1 and 2) amplitudes and Eliassen-Palm (E-P) fluxes in the lower stratosphere, and find that the wave activity has not declined in recent decades. To reconcile with the speculation by a number of authors that the vertical propagation of the planetary waves should be impeded, we clarify a possible confusion related to the effect of vertical wind shear on the upward propagation of planetary waves. In section 4, we first re-establish the dynamical control in the year-to-year variations of polar mean temperatures. We then study the relationship between dynamical heating and January-mean polar mean temperatures on both interannual and decadal timescales. In section 5, we study the relationship of planetary waves and stratospheric cooling on the zonal-mean state represented by angular momentum and the NAM index. A summary of principal conclusions, together with some speculations, is provided in section 6.

2. Data

The data used in this study is the reanalysis data from the National Center for Environmental Prediction/National Center for Atmospheric Research (NCEP/NCAR). Wavenumber 1 and 2 are Fourier decomposed from 51-year (November, 1949 - January, 2000) geopotential heights. To avoid dealing with the boundary problems of the NCEP/NCAR reanalysis model, our analysis does not go above 20 mb. The daily data of 41-year (1958-1998) NAM index at 50 mb, computed from the NCEP/NCAR data, were provided by Mark Baldwin. Detailed information of the NAM index can be found in Baldwin and Dunkerton (1999) and Baldwin and Dunkerton (2001). There are three time lines that must be noted in linear trend statistics. The reanalysis data at stratospheric levels before 1958 are probably not reliable due to the lack of sufficient observational data in the upper atmosphere. In many recent works, 1968 is the year that is considered the starting year for stratospheric cooling and for the positive trend in NAM index. Satellite data have been included in generating the reanalysis data since 1979.

3. Trends of planetary-wave activity

3.1. Planetary-wave amplitudes

We first examine the long-term variations of planetary-wave amplitudes in the stratosphere. Figure 1 illustrates the variability of wavenumber-1 amplitudes, averaged over NDJ, at 200, 100, 50, and 20 mb along the 60°N latitude circle (amplitudes averaged over December-February is nearly the same as that over NDJ). On interannual timescales, wavenumber-1 amplitude varies substantially, and the variations at the four levels are vertically coherent. Focusing now on the decadal trends, wavenumber-1 amplitudes increase significantly from 1958 to 2000 (amplitudes before 1958 are unrealistically small). At 20 mb, the net increase in amplitude is about 93 meters in the 43 years. This is a rather large increase compared with the 43-year mean amplitude of 433 meters (thus about 20%

of the mean). The linear trends in wave amplitudes at 20 and 50 mb are about 2.18 and 1.45 m/yr, at significance levels above 97.5% and 99%, respectively. The trends vary with latitudes, with the largest slope near 60°N. There are no significant trends at 100 and 200 mb. For periods of 1968-2000 and 1979-2000, wave amplitudes at all 4 levels do not show significant trends, though wave amplitudes increase at 20 mb and slightly decrease at 200 mb. Additional calculations show that there are no significant trends in wavenumber-1 amplitudes at levels below 200 mb. NDJ-mean wavenumber-2 amplitudes are showed in Figure 2. The amplitudes at all the four levels exhibit no statistically significant trends in any of the three periods: 1958-2000, 1968-2000, and 1979-2000.

One can conclude that in the NCEP/NCAR data there is no evidence for a decrease in planetary-wave amplitudes in the lower stratosphere in the past 51 or 43 years. If any thing a case can be made that wavenumber-1 amplitudes have increased at some levels.

3.2. Eliassen-Palm flux

In this subsection, we study the evolution of the E-P flux from the troposphere to the stratosphere in the past few decades since it is the E-P flux and its convergence that measure the overall irreversible wave driving of residual meridional circulation and dynamical heating in the stratosphere.

Following Dunkerton and Baldwin (1991) and Salby et al. (2000), we first define a box from 50°N to 90°N in latitude and from 100 to 20 mb in height. For the space covered by this box, E-P flux across 100mb (F_{100mb}) measures the overall wave activity coming from the troposphere, E-P flux across 20 mb (F_{20mb}) is the amount going into the upper stratosphere, and E-P flux across the boundary of 50°N ($F_{50^\circ N}$) is the meridional flux out of the box. The combination of the three components, i.e. $F_{net} = F_{20mb} - F_{100mb} - F_{50^\circ N}$ is the "net" E-P flux out of this box, which presents the total E-P flux divergence. In each year, E-P flux is averaged over three-months (NDJ). In calculating E-P flux, the quasi-geostrophic version of E-P flux in spherical geometry is used (Edmon et al., 1980, Andrews, Holton, and

Leovy, 1987). Figure 3 shows F_{100mb} (dotted line), F_{20mb} (dash-dot line), $F_{50^\circ N}$ (dash line), and F_{net} (solid line) for the 51 years. Similar to the results by Fusco and Salby (1999) and Salby et al. (2000), the upward E-P flux across 100 mb has large interannual variabilities. Comparison of F_{100mb} with F_{20mb} suggests that about half of the upward E-P flux penetrates the top of the box and goes into the upper stratosphere. Negative net E-P flux means that planetary-wave activity always tends to decelerate the westerly mean flow. The most important point to note here is that the plots do not exhibit evidence of either decreasing E-P flux from the troposphere or decreasing E-P flux divergence in the past 51 years.

3.3. Vertical wind shear in the upper troposphere

The results presented in the last two subsection do not seem to be consistent with the notion that the stratospheric cooling in the past few decades should be associated with a decline in wave activity in the stratosphere. It also seems to contradict the speculation that the wave propagation from the troposphere to the stratosphere should be impeded by the increase in vertical shear near the tropopause level by the greenhouse warming effects. We would like in this subsection clarify some possible confusion in recent literature on the effect of vertical shear on the upward propagation of planetary waves, and reconcile the theory with the observation.

From linear wave theory (Charney and Drazin, 1961; Andrews, Holton, and Leovy, 1987), it is well known that upward propagation of planetary waves from the troposphere into the stratosphere is mediated by the basic flow, $\bar{u}(y,z)$. Specifically, the capability for wave propagation is characterized by the square of the index of refraction which, in the spherical quasi-geostrophic form, is given by

$$n_k^2(y,z) = \frac{\bar{q}_\phi}{\bar{u} - (a\sigma\cos\phi)/k} - \left(\frac{k}{a\cos\phi}\right)^2 - \left(\frac{f}{2NH}\right)^2, \tag{1}$$

where

$$\bar{q}_\phi = \frac{2\Omega}{a}\cos\phi - \frac{1}{a^2}\left[\frac{(\bar{u}\cos\phi)_\phi}{\cos\phi}\right]_\phi - \frac{f^2}{\rho_0}\left(\rho_0\frac{\bar{u}_z}{N^2}\right)_z \tag{2}$$

is the meridional potential vorticity (PV) gradient. Here, k, σ, N, H, f, ρ_0, a, Ω, and ϕ denote the zonal wavenumber, wave frequency, buoyancy frequency, scale height, Coriolis parameter, background air density, Earth's radius, Earth's rotation frequency, and latitude, respectively. It is expected that planetary waves are able to propagate in regions where $n_k^2 > 0$ and are refracted from regions where $n_k^2 < 0$, and that the larger the n_k^2 in a region, the easier it is for planetary waves to propagate there (Matsuno, 1970).

As pointed out by Limpasuvan and Hartmann (2000), it is the third term on the right-hand side of (2) that accounts for the largest variation of the refractive index. Expansion of this term yields

$$-\frac{f^2}{\rho_0}\left(\rho_0\frac{\bar{u}_z}{N^2}\right)_z = \left(\frac{f^2}{HN^2} + \frac{f^2}{N^4}\frac{dN^2}{dz}\right)\bar{u}_z - \frac{f^2}{N^2}\bar{u}_{zz}. \tag{3}$$

Here, we have applied $\rho_0(z) = \rho_s \exp\left(-\frac{z}{H}\right)$ and will assume $\frac{dN^2}{dz} > 0$. The first term on the right-hand side of (3), involving $\bar{u}_z$, is the dominant one, except near the jet maximum. Substituting this into (2) and combining with (1), one can find that a larger vertical wind shear $\bar{u}_z$ should enhance meridional PV gradients and lead to a larger n_k^2 and thus enhances upward propagation of planetary waves, rather than refracting them (Tung and Lindzen, 1979). From the thermal wind relation, $\frac{\partial \bar{u}}{\partial z} = -\frac{R}{Hf}\frac{\partial \bar{T}}{\partial y}$, it then follows that an increase in the north-south temperature gradient ($-\frac{\partial \bar{T}}{\partial y}$) in the upper troposphere, as noticed by Rind et al. (1998), Shindell et al. (1998), and Shindell et al. (1999) in their simulations, should lead to an enhancement of the upward propagation of planetary waves, rather than suppressing it. In fact, Rind et al. (1998) found that doubling CO_2 leads to an increase of large-scale eddy energy and residual circulation in the stratosphere.

The work by Chen and Robinson (1992) dealt with negative vertical wind shears near the tropospause. When a negative shear anomaly is superimposed on their standard wind profile (it makes the vertical shear near the tropopause more negative), they found that E-P flux convergence was reduced by as much as 20% in the stratosphere in high latitudes and as much as 40% in the upper tropospheric polar region. Therefore, their conclusion

that smaller (less negative) vertical wind shear enhances wave propagation crossing the tropopause is consistent with ours.

Figure 4a illustrates the vertical wind shears of zonal mean zonal wind in the upper troposphere (250 mb), averaged over NDJ, as a function of years. This level is the one considered by Rind et al. (1998), Shindell et al. (1998) and Shindell et al. (1999). At this level the tropics is warm, while middle and high latitudes are cold. Because of the strong meridional temperature gradient between 30°N to 40°N, the vertical shear at 35°N is about three times larger than the vertical shears at 45°N, 55°N, and 65°N. The shear at 35°N has a positive trend from 1958 to 2000, with a slope of 0.004 $ms^{-1}km^{-1}/yr$ and significance above 99.99%. From 1968 to 2000, the trend is also about 0.004 $ms^{-1}km^{-1}/yr$, with significance above 95%. From 1979 to 2000, the shear is slightly increasing, but not significant. This appears to be consistent with the suggestion by Shindell et al. (1998), Limpasuvan and Hartmann (2000), and Hartmann et al. (2000), as far as the vertical shear is concerned. Vertical shears at 45°N, 55°N, and 65°N do not show any significant trends.

Figure 4b shows the vertical wind shear near the tropopause (100 mb). Shears at 35°N and 45°N show negative values because the tropics becomes cold, while middle latitudes are relatively warm. This is the case studied by Chen and Robinson (1992). The vertical shear at 35°N has significant trends from 1958 to 2000 and from 1968 to 2000, with slopes of about $0.01ms^{-1}km^{-1}/yr$ and $0.008ms^{-1}km^{-1}/yr$ and significance above 99.5%. From 1979 to 2000, the vertical shear does not show a significant trend, though it still increases (becomes less negative). No significant trends are found for vertical shears at other latitudes.

Therefore, from the data on vertical shears and from the argument on the effect of vertical shears on the index of refraction, there is no evidence that planetary waves propagation into the stratosphere should be suppressed in the past few decades.

4. Relation between dynamical heating and stratospheric cooling

4.1. Theoretical considerations

Before we present more observational results, it is necessary to show theoretically the relationship between planetary-wave fluxes and the dynamical heating of the zonal mean state, because there have been some confusion on this relationship also.

Under the quasi-geostrophic approximation applicable to the extratropical region, the zonal mean temperature equation is (see page 129, Andrews, Holton, and Leovy, 1987):

$$\frac{\partial \bar{\theta}}{\partial t} = -\theta_{0z}\bar{w}^* + \bar{Q}, \tag{4}$$

where $\theta \equiv T\left(\frac{p_0}{p}\right)^{\frac{R}{C_p}}$ is the potential temperature, $\theta_{0z} = \frac{d\theta_0}{dz}$ is the vertical gradient of the background state of the potential temperature, $\bar{\theta}$ is the zonal mean potential temperature, $\bar{w}^*$ is the vertical velocity component of the transformed Eulerian mean circulation, and $\bar{Q}$ is the zonal mean net radiative heating. The first term on the right-hand side of equation (4) is the so-called dynamical heating induced by adiabatic compression of descending motion in the polar region. It is related to the residual meridional motion through the continuity equation

$$\frac{\partial}{\partial y}(\rho_0 \bar{v}^* \cos\phi) + \frac{\partial}{\partial z}(\rho_0 \bar{w}^*) = 0, \tag{5}$$

with $y = asin\phi$.

The nondivergent nature of the meridional circulation (5) implies the existence of a streamfunction Ψ such that

$$\rho_0 \bar{v}^* \cos\phi = -\frac{\partial \Psi}{\partial z}, \qquad \rho_0 \bar{w}^* = \frac{\partial \Psi}{\partial y}. \tag{6}$$

Let $<\quad>$ denote area-weighted meridional average from a latitude ϕ to the pole, i.e.,

$$\langle A \rangle = \frac{\int_\phi^{\frac{\pi}{2}} Aa\cos\phi d\phi}{\int_\phi^{\frac{\pi}{2}} a\cos\phi d\phi} = \frac{\int_\phi^{\frac{\pi}{2}} A\cos\phi d\phi}{(1-\sin\phi)}. \tag{7}$$

Equation (4) becomes, assuming that Ψ vanishes at the pole,

$$\frac{\partial}{\partial t}\left\langle \rho_0 \bar{\theta} \right\rangle = \frac{\theta_{0z}\Psi|_\phi}{a(1-\sin\phi)} + \left\langle \rho_0 \bar{Q} \right\rangle. \tag{8}$$

The quasi-geostrophic form of the zonal momentum equation is

$$\frac{\partial \bar{u}}{\partial t} - f\bar{v}^* = \frac{1}{\rho_0(z)} \bigtriangledown \cdot \mathbf{F}, \tag{9}$$

where $\bigtriangledown \cdot \mathbf{F} = \frac{\partial}{\partial y}(-\rho_0 \overline{u'v'} \cos\phi) + \frac{\partial}{\partial z}(\frac{\rho_0 f}{\theta_{0z}} \overline{v'\theta'})$ is the Eliassen-Palm flux divergence, which embodies the irreversible, net effect of wave activity on the mean flow. Under seasonal time averaging, the dominant balance in (9) is between the Coriolis torque and the wave driving

$$-f\rho_0\bar{v}^* = \bigtriangledown \cdot \mathbf{F}, \tag{10}$$

which is the same as

$$\frac{f}{\cos\phi}\frac{\partial \Psi}{\partial z} = \bigtriangledown \cdot \mathbf{F}. \tag{11}$$

Integrating (11) with respect to z yields

$$\Psi = \frac{\rho_0}{\theta_{0z}} \overline{v'\theta'} \cos\phi + \delta, \tag{12}$$

where $\delta = -\frac{1}{af}\frac{\partial}{\partial\phi}\int_z^\infty \rho_0 \overline{u'v'} \cos\phi dz$. For z in the lower stratosphere, δ is found from our calculations to be small compared to the first term on the right-hand side of (12). Figure 5 shows the three-month mean of the two quantities. The quantity, δ, which is determined by the horizontal momentum flux divergence, is about 2 orders of magnitude smaller than the term related to heat flux. Consequently, (8) becomes, to a high degree of accuracy,

$$\frac{\partial}{\partial t}\left\langle \bar{\theta} \right\rangle \approx \left. \frac{\overline{v'\theta'} \cos\phi}{a(1-\sin\phi)} \right|_\phi + \left\langle \bar{Q} \right\rangle. \tag{13}$$

We see that at level z the dynamical heating for the mean temperature averaged over an area from latitude ϕ to the north pole is given by the poleward heat flux $\overline{v'\theta'} \cos\phi$ at latitude ϕ. Note that the dynamical heating is neither directly given by E-P flux divergence, $\bigtriangledown \cdot \mathbf{F}$, nor by latitudinally integrated upward E-P flux across the tropopause (Fusco and Salby, 1999), F_{100mb}, nor by the momentum flux (Limpusavan and Hartmann, 2000). Integrating (13) with respect to altitudes then yields the relationship between column-averaged temperature and dynamical heating on the column. The derivation can also be given from the Eulerian mean temperature equation with perhaps a little more ease.

Equation (13) provides a way for quantifying the relationship between the mean polar temperature and wave-driven dynamical heating as well as radiative cooling. For our interest in the present paper, we focus on the qualitative relationship between the January-mean polar mean temperature and the dynamical heating. Integrating (13) from November to January gives

$$\left\langle \bar{\theta} \right\rangle_{Jan.} - \left\langle \bar{\theta} \right\rangle_{Nov.} = \int_{Nov.}^{Jan.} F_{\phi,z} dt + \int_{Nov.}^{Jan.} \left\langle \bar{Q} \right\rangle dt, \tag{14}$$

where

$$F_{\phi,z} = \frac{\overline{v'\theta'} \cos\phi}{a(1-\sin\phi)}\Big|_{\phi} \tag{15}$$

denotes the poleward heat flux at latitude ϕ and z. (14) means that $\left\langle \bar{\theta} \right\rangle_{Jan.}$ (or the difference between it and $\left\langle \bar{\theta} \right\rangle_{Nov.}$) is determined by cumulative dynamical heating during preceding months, as suggested by Salby et al. (2000). In the next subsection, we shall show the correlation between $F_{60^\circ N,50mb}$ and $\left\langle \bar{\theta} \right\rangle_{Jan.}$.

4.2. Dynamical heating vs. temperature

Let us first look at the temperature evolution in the lower stratosphere during the past 51 years. Figure 6 illustrates January-mean polar temperatures at 5 levels: 100, 70, 50, 30, and 20 mb, area-weighted over 60°N-90°N, as a function of years. The temperatures are vertically coherent and exhibit large interannual variations, ranging from 200 to 220 K. On decadal timescales, the temperatures at all the levels show significant negative trends from 1968 to 2000. At 50 mb, the trend is about -0.17 K/yr at significance level above 97.5%. The polar mean temperature at 50 mb reaches a minimum of 201 K in January, 2000. The net decrease of the polar mean temperature is about 5.6 K in the past 33 years. This result is consistent with the stratospheric cooling trend for winter-spring of -5 $K/(19\ yr)^{-1}$ reported by Pawson et al. (1998), Randel and Wu (1999), and Thompson et al. (2000) from the Microwave Sounding Unit channel-4 (MSU-4) data. Randel and Wu (1999) in particular found a -4 to -8 K Arctic cooling during January-April (peaking in spring) since

1985. The smaller cooling trend in our result is probably because ozone depletion is not yet a large factor for Arctic cooling during polar night (e.g. January), unlike the case after the final warming. Note that the significance of the trend is sensitive to the starting year chosen because of the large interannual variability. For example, if one chooses the starting year after 1970, one will not find a significant trend.

In the summer season, the stratosphere is dynamically less disturbed, and hence has temperatures close to radiative equilibruim. Therefore, any temperature trend induced by radiative cooling should be more readily detected from summer temperatures. To verify whether a cooling trend exists in the Arctic polar region, we have calculated July mean temperatures, averaged over the same polar region, at the 5 levels. The results are plotted in Figure 7. Compared to that of the January mean temperatures, the interannual variabilities of the July mean temperatures are much smaller, within 3 K at each level. The temperatures first increase, reaching maximum in July, 1968. It then monotonically decreases to year 2000 at 100, 70, and 50 mb. As marked in the figure, the trends at these levels from 1979 to 2000 are about -0.06, -0.07, and -0.05 K/yr, respectively, with significance all close to 100% (values in the bracket are student's t-test values). The trends are close to the results from CLIMAT TEMP data reported by Gaffen et al. (2000). At 30 mb, the temperature does not show a significant trend. A warming trend is found at 20 mb, with significance above 90%. Randel and Wu (1999) and Gaffen et al. (2000) also showed similar warming trends at levels above 30 mb. It seems that stratospheric cooling is mainly in the lower stratosphere. Compared to the trends in winter, the cooling trends during summer seasons are more systematic and significant.

Though the winter trends is not as systematic as the summer trend, the long-term temperature variation in winter is not inconsistent with the summer trend. For example, if one calculates the winter trend starting from 1977, one would obtain a trend with a slope of -0.05 K/yr (circle-dash line in Figure 6), which is close to the summer trend.

To examine the relationship between temperature and dynamical heating due to planetary waves, in Figure 8 we plot the anomalies of the January-mean polar mean temperature, as a function of years, against the normalized anomalies of heat flux $F_{60^\circ,50mb}$ averaged over the three preceding months (NDJ). Consistent with the prediction in (13) or (14), the interannual variability of the temperature is indeed driven by the interannual variability of the cumulative wave-driven heat flux in the preceding months. For the period from 1958 to 2000, the correlation coefficient between the two is about 0.73 (the nearly anti-correlation before 1958 appears to be due to bad data). From 1968 to 2000, the correlation is about 0.90. From 1979 to 2000, the correlation is about 0.84. These are all very high correlation coefficients. The correlation of interannual variations between the polar mean temperature at 50 mb and $F_{60^\circ N,50mb}$ is very close to that between the column-averaged (100-10mb) polar temperature and F_{100mb} in Salby et al. (2000).

Though there is a strong correlation of interannual variations between the polar mean temperature and wave driven heat flux $F_{60^\circ N,50mb}$, the two appear to behave differently on longer timescales. From Figure 8, one can see that the long-term trends of the two diverge. The trend in the temperature is steep and statistically significant, while the linear regression of $F_{60^\circ N,50mb}$ has a nearly zero slope (note that the linear regression of $F_{60^\circ N,50mb}$ (dashed line) is not a statistically significant trend. It is plotted for comparison with the trend in temperature. The same is true for the linear regression of F_{100mb} in following figures). This suggests that the stratospheric cooling is probably a result of radiative cooling, i.e. $\left\langle \bar{Q} \right\rangle$ in (13), possibly due to greenhouse gas effects, rather than a result of a decrease of dynamical heating induced by planetary waves.

To compare with the result by Salby et al. (2000), in Figure 9 we plot the normalized anomalies of $F_{60^\circ N,50mb}$, against the NDJ-mean overall upward E-P flux from the troposphere, F_{100mb}. Except in few years when the two are out of phase (e.g. 1958, 1974), the interannual variations of $F_{60^\circ N,50mb}$ and F_{100mb} are very consistent. From 1968 to

2000, their correlation coefficient is about 0.80. This is not surprising because $F_{60^\circ N,50mb}$ is part of the overall planetary-scale wave driving from the troposphere.

As mentioned above, the cooling trend in the January-mean polar mean temperature is about three times larger than the summer cooling trend. The large interannual variation of dynamical heating may affect the linear trend obtained for winter. In order to reduce the influence of the interannual variations of dynamical heating on the cooling trend, we use the method of least-squares regression by minimizing the sum of squared residual

$$\sum_{i=1}^{33} \left(T_{50mb}(t_i) - \alpha F_{60^\circ N,50mb}(t_i) - b - \gamma t_i\right)^2, \tag{16}$$

where, γ is the trend we expect after reducing fluctuations of dynamical heating, α is the optimized coefficient for reducing fluctuations from $F_{60^\circ N,50mb}$, and t_i denotes years. Figure 10 illustrates normalized T_{50mb}, $F_{60^\circ N,50mb}$, $T_{50mb} - \alpha F_{60^\circ N,50mb}$, and $b + \gamma t_i$. One sees that fluctuations of $T_{50mb} - \alpha F_{60^\circ N,50mb}$ (solid line) are less than these of T_{50mb} (dotted line). The trend for normalized $T_{50mb} - \alpha F_{60^\circ N,50mb}$ is $\gamma \approx -0.29$. Transforming it to the unnormalized case gives $\frac{\gamma \sigma_{T_{50mb}}}{\sigma_t} = \frac{-0.29 \times 4.6}{9.8} \approx -0.14\ K/yr$ with significance above 97.5%, where $\sigma_{T_{50mb}}$ and σ_t are the standard deviations of T_{50mb} and $b + \gamma t_i$. The obtained winter cooling slope does not change very much even after the interannual fluctuations of dynamical heating are minimized. Nevertheless, visually it is clearer from Figure 10 that there is a downward slope in $T_{50mb} - \alpha F_{60^\circ N,50mb}$ (solid line).

5. E-P flux vs. NAM index and angular momentum

Now we turn attention to the relationship planetary-wave activity and the zonal-mean flow. Since the NAM index consists mostly of the anomalies of zonal mean geopotential heights, it can be considered to be representative of the zonal mean state. Hence the positive trend of the NAM index is consistent with the strengthening polar night jet (Thompson and Wallace, 1998; Wallace, 2000), which is in turn consistent with the polar cooling.

Figure 11 shows the normalized anomalies of the January-mean NAM index at 50 mb

as a function of years, against F_{100mb}. On interannual timescales, F_{100mb} and the NAM index have an anti-phase relationship, with a rather high correlation coefficient of about -0.73. The correlation becomes stronger for more recent years probably because of better data. For the periods: 1968-1998 and 1979-1998, the correlation coefficients are -0.78 and -0.88, respectively. On decadal timescales, the evolution of the two becomes divergent. The NAM index shows a significant positive trend over 1968-1998, with slope 0.04 yr^{-1} and confidence close to 95%. This result was first obtained by Thompson et al. (2000). Over the same period, the linear regression of F_{100mb} has a slope that is not statistically different from zero.

In Limpasuvan and Hartmann (1999, 2000) and Hartmann et al. (2000), the authors particularly focused on the interaction between the NAM index and eddy-momentum flux (which is equivalent to the horizontal component of the E-P flux here). To demonstrate the long-term relationship between the horizontal E-P flux and the NAM index, in Figure 12 we re-plot the NAM index together with normalized $F_{50^\circ N}$ (the latter was already shown in Figure 3). The two are generally anti-correlated on interannual timescales, and the anti-correlation is as good as that for the vertical E-P flux in Figure 11. Their long-term trends are more significantly divergent compared to those in Figure 11 for the vertical flux. This also suggests that the long-term trend in the NAM index is not coupled with that of wave E-P flux. (Incidentally, it should be noted that in the stratosphere, the momentum flux is not an important factor in the momentum budget; see Figure 3).

In Limpasuvan and Hartmann (1999, 2000) and Hartmann et al. (2000), the E-P flux vectors were composited according to the high-low phases of NAM indices on a winter-to-winter basis. Thus, what was found by them actually represents the interannual relationship between the NAM index and the E-P flux vectors. The anti-correlation between the NAM index and the E-P flux shown above reflects this relationship on interannual timescales. It suggests that the dynamical heating caused by the upwelling wave E-P flux

and the thermal wind relationship can account for most of the year-to-year variations of the NAM index (treating the latter as a zonal mean quantity). Over decadal timescales, however, the positive trend in the NAM index, which is consistent with a decreasing polar mean temperature, is not explainable by the E-P flux trend, which is nearly zero. We thus suggest that the positive trend in the NAM index is probably caused by radiative effects, a different mechanism from that causing the interannual high NAM index phases.

The interaction between planetary waves and the zonal mean state in the stratosphere can also be demonstrated in the zonal mean angular momentum budget. From the transformed Eulerian-mean momentum equation, Tung (1986) and Dunkerton and Baldwin (1991) have deduced that the tendency of zonal-mean angular momentum over a time period is approximately given by the E-P flux divergence averaged over the simultaneous period, that is,

$$\frac{\partial \langle M \rangle}{\partial t} \approx F_{net} - \langle X \rangle \,, \tag{17}$$

where $M = \rho_0 a \cos\phi(\bar{u} + \Omega a \cos\phi)$ is the angular momentum, $\langle M \rangle = \int_{z1}^{z2} \int_{\phi_1}^{\frac{\pi}{2}} M a \cos\phi d\phi dz$ is the mean angular momentum integrated over latitude and height, and $\langle X \rangle$ represents the mean advection of M. However, we found that zonal-mean angular momentum does not correlate with E-P flux divergence as well as its correlation with the upward E-P flux, F_{100mb}. It is probably because the mean advection of angular momentum $\langle X \rangle$ is not negligible. Instead, we shall focus on the correlation between angular momentum tendency and F_{100mb}, since the latter measures the overall wave driving coming from the troposphere, as pointed out by Salby et al. (2000).

Figure 13 shows normalized anomalies of angular momentum difference between January-mean and November-mean as a function of years, against normalized F_{100mb} anomalies (Angular momentum is averaged over the same box as that for E-P flux in Figure 3). Similar to the relationship between the NAM index and E-P flux, the angular momentum difference and upward E-P flux are also anti-correlated on interannual

timescales. From 1958 to 2000, the correlation coefficient is about -0.72. For periods of 1968-2000 and 1979-2000, the correlation coefficients are -0.82 and -0.85, respectively. Such strong anti-correlations mean that the interannual variability of angular momentum tendency is coupled with planetary-wave activity. Again, the two show different trends for longer-time scales. The angular momentum difference has a significant trend over the period of 1968-2000, with a slope of about $2.0 \times 10^8\ kg\ ms^{-1}/yr$ and significance close to 95%, in contrast to the nearly zero slope of the linear regression of F_{100mb}. This also suggests that it is not the upwelling wave E-P flux which causes the increase in zonal mean angular momentum.

6. Conclusions

Using 51-year NCEP/NCAR reanalysis data, we have studied the interannual and long-term variations of planetary-wave activity and stratospheric cooling. Our results demonstrate that there is no evidence indicating a decrease of planetary-wave activity from the troposphere into the stratosphere. Both E-P flux across the tropopause and planetary-wave amplitudes in the lower stratosphere do not show significant changes in the past few decades. This disagrees with the speculation that planetary-wave activity in the stratosphere might have been reduced by altered climate conditions in the upper troposphere due to the greenhouse effect. We clarify that stronger vertical zonal-wind shears should enhance upward propagation of planetary waves, rather than refracting them.

Our results show that on interannual timescales the variation of the January-mean polar mean temperature is strongly driven by poleward heat flux (which is coherent with the upward E-P flux across 100 mb). On timescales of decades, however, the two are not coupled. The temperature has a significant cooling trend in the recent 30 years, while both the poleward heat flux and the upward E-P flux across 100 mb do not have any significant trend. This suggests that the cooling trend in the polar temperatures is probably a result

of radiative cooling, due possibly to the greenhouse effect and/or ozone depletion, and not a result of declining planetary wave activity.

Similarly, on interannual timescales the variabilities of the NAM index and angular momentum are all strongly anti-correlated with the interannual variability of the upward E-P flux across 100 mb. For longer timescales, the significant, positive trends in the NAM index and angular momentum during the last 30 years are not accompanied by a decrease of the upward E-P flux from the troposphere. Therefore, these positive trends can also be attributed to radiative cooling. An evidence that may support this argument is that the NAM trend is most significant in the lower stratosphere (Hartmann et al., 2000), where the cooling trend in the polar mean temperature is also the most significant, as shown in Figure 7.

In the present paper, we have mainly focused on the variations of planetary waves, polar mean temperature and NAM in early and middle winter. We have not touched upon the issue of stratospheric cooling in late winter and spring. As briefly mentioned above, stratospheric cooling trends in early vs late winter are very different due to the radiative effect of ozone, which becomes more important during and after the final warming, when the sun returns. It has also been suggestted that recent stratospheric cooling in late winter and early spring might be partly attributed to less ozone transport from the tropics to the Arctic polar region due to a decrease of planetary wave activity (Coy et al., 1997, Shindell et al. 1998). Whether or not this speculation is true, given the evidence to the contrary for early winter, remains to be addressed.

Acknowledgments. We are grateful to James Holton, Dennis Hartmann, and Walter Robinson for their comments on an early draft of this paper. We have benefited from many discussions with Katie Coughlin. We also thank Mark Baldwin, who provided us with the data of the NAM index. NCEP Reanalysis data is provided by the NOAA-CIRES Climate Diagnostics Center, Boulder, Colorado, USA, from their Web site at http://www.cdc.noaa.gov/. This work

is supported by the National Science Foundation, Division of Atmospheric Sciences, Climate Dynamics, under grant ATM 9813770.

References

Andrews, D. G., J. R. Holton, and C. B. Leovy, 1987: *Middle Atmosphere Dynamics*, Academic Press, New York, p. 489.

Baldwin, M. P., and T. J. Dunkerton, 1999: Propagation of the Arctic Oscillation from the stratosphere to the troposphere. *J. Geophys. Res.,* **104 ,** 30937-30946.

Baldwin M. P., and T. J. Dunkerton, 2001: Changes in weather patterns following stratospheric circulation anomalies. Submitted to *Nature,* .

Charney, J. G., and P. G. Drazin, 1961: Propagation of planetary-scale disturbances from the lower to the upper atmosphere, *J. Atmos. Sci.,* **66**, 83-109.

Chen, P. and W. A. Robinson, 1992: Propagation of planetary waves between the troposphere and stratosphere. *J. Atmos. Sci.,* **51,** 2533-2545.

Coy, L., E. R. Nash, and P. A. Newman, 1997: Meteorology of the polar vortex: Spring 1997. *Geophys. Res. Lett.*, **13**, 1221–1223.

Dunkerton, T. J., and M. P. Baldwin, 1991: Quasi-biennial modulation of planetary-wave fluxes in the Northern Hemisphere winter. *J. Atmos. Sci.,* **48**, 1043-1061.

Edmon, H. J. Jr., B. J. Hoskins, and M. E. McIntyre, 1980: Eliassen-Palm cross sections for the troposphere. *J. Atmos. Sci.,* **37**, 2600-2616.

Fusco, A. C., and M. L. Salby, 1999: Interannual variations of total ozone and their relationship to variations of planetary wave activity. *J. Climate,* **12**, 1619-1629.

Gaffen, D. J., M. A. Sargent, R. E. Habermann, and J. R. Lanzante, 2000: Sensitivity of tropospheric and stratospheric temperature trends to Radiosonde data quality. *J. Climate*, **13**, 1776–1796.

Gillett, N. P., G. C. Hegerl, M. R. Allen, and P. A. Stott, 2000: Implications of observed changes in the Northern Hemisphere circulation for the detection of anthropogenic climate change. *Geophys. Res. Lett.,* **27,** 993-996.

Hartmann, D. L., J. M. Wallace, V. Limpasuvan, D. W. J. Thompson, and J. R. Holton , 2000:

Can ozone depletion and greenhouse warming interact to produce rapid climate Change? *Proc. Nat. Acad. Sci.,* **97**, 1412-1417.

Labitzke, K., and B. Naujokat, 2000: The lower Arctic stratosphere in winter since 1952, *SPARC Newsletter,* **15**.

Limpasuvan, V., and D. L. Hartmann, 1999: Eddies and the annular modes of climate variability. *Geophys. Res. Lett.,* **26,** 3133-3136.

Limpasuvan, V., and D. L. Hartmann, 2000: Wave-maintained annular modes of climate variability, *J. Climate,* , **13**, 4414-4429.

Matsuno, T., 1970: Vertical propagation of stationary planetary waves in the winter northern hemisphere. *J. Atmos. Sci.,* **27**, 871-883.

Newman, P. A., J. F. Gleason, R. D. McPeters, and R. S. Stolarski, 1997: Anomalously low ozone over the Arctic. *Geophys. Res. Lett.,* **24**, 2689-2692.

Pawson, S., K. Labitzke, and S. Leder, 1998: Stepwise changes in stratospheric temperature. *Geophys. Res. Lett.,* **25**, 2157-2160.

Randel, W. J., and F. Wu, 1999: Cooling of the Arctic and Antarctic polar stratospheres due to ozone depletion. *J. Climate,* **12,** 1467-1479.

Rind, D., D. T. Shindell, P. Lonergan, and N. K. Balachandran, 1998: Climate change of the middle atmosphere. Part III: The doubled CO_2 climate revisited. *J. Climate,* **11,** 876-894.

Salby, M., P. Callaghan, P. Keckhut, S. Godin, and M. Guirlet, 2000: Interannual changes of temperature and ozone. *SPARC Newsletter,* **15**.

Shindell, D. T., Rind, D., P. Lonergan, 1998: Increased polar stratospheric ozone losses and delayed eventual recovery due to increasing greenhouse gas concentrations. *Nature*, **392**, 589-592.

Shindell, D. T., R. L. Miller, G. A. Schmidt, and L. Pandolfo, 1999: Simulation of recent northern climate trends by greenhouse-gas forcing, *Nature*, **399**, 452-455.

Thompson, D. W. J., and J. M. Wallace, 1998: The Arctic Oscillation signature in the wintertime geopotential height and temperature fields. *Geophys. Res. Lett.,* **25,** 1297-1300.

Thompson, D. W. J., J. M. Wallace, and G. C. Hegerl, 2000: Annular modes in the extratropical circulation. Part II: Trends. *J. Climate,* **13**, 1018-1036.

Tung, K. K., 1986: Nongeostrophic theory of zonally averaged circulation, Part I: Formulation, *J. of Atmos. Sci.*, **43**, 2600-2618.

Tung, K. K., and R. S. Lindzen, 1979: A theory of stationary long waves, Part II: Resonant Rossby waves in the presence of realistic vertical shears, *Mon. Wea. Rev.,* **107,** , 735-750.

Wallace, J. M., 2000: North Atlantic Oscillation/Northern Hemisphere annular mode, One phenomenon, two paradigms. *Q. J. Roy. Met. Soc.,* in press.

Waugh, D. W., W. J. Randel, S. Pawson. P. A. Newman, and E. R. Nash, 1999: Persistence of the lower stratospheric polar vortices. *J. Geophys. Res.,* **104,** 27191-27202.

Yongyun Hu and Ka Kit Tung, Department of Applied Mathematics, University of Washington, Seattle, WA 98195. (e-mail: yongyun@amath.washington.edu; tung@amath.washington.edu)

Received _____

Figure captions

Figure 1: NDJ mean wavenumber-1 amplitudes at four levels along the 60°N latitude circle. Solid line: 20 mb, dash-dot line: 50 mb, dashed line: 100 mb, dotted line: 200 mb.

Figure 2: Same as Figure 1, except for wavenumber 2.

Figure 3: Plots of NDJ-mean total upward E-P flux at 100mb (dotted line) and 20mb (dash-dot line), total horizontal E-P flux across the box boundary from 100 mb to 20 mb at 50°N (dashed line), and the net E-P flux (solid line) in the box.

Figure 4: Vertical shears of zonal mean zonal wind, averaged over NDJ, at 250 mb (a) and 100 mb (b). Each plot shows wind shears at four latitudes, 35°N (solid line), 45°N (dash-dotted line), 55°N (dotted line), and 65°N (dashed line). The shears at 250 mb are averaged from the vertical shears between 200 and 250 mb and that between 250 and 300 mb. The shears at 100 mb are averaged from the shears between 70 and 100 mb and that 150 and 100 mb.

Figure 5: Comparison of magnitudes between eddy heat flux and eddy momentum flux divergence at 50 mb and 60°N.

Figure 6: January-mean temperatures at 100, 70, 50, 30, and 20 mb, area-weighted over 60°N-90°N, as a function of years. Legends are marked in the plot.

Figure 7: July-mean temperatures at 100, 70, 50, 30, and 20 mb, area-weighted over 60°N-90°N, as a function of years. Legends are marked in the plot.

Figure 8: Anomalies of January-mean temperature at 50mb, averaged over 60°N-90°N, vs. years, against normalized poleward heat flux, $F_{60^\circ N,50mb}$ (normalized by its root-mean-square (RMS)). The dash-dot line is the trend in temperature, and the dashed line is the linear regression of $F_{60^\circ N,50mb}$. For comparing with the temperature anomaly, the normalized E-P flux is multiplied by 5.7.

Figure 9: Comparison of normalized anomalies of $F_{60^\circ N,50mb}$ with normalized total upward E-P flux F_{100mb}.

Figure 10: Cooling trend in January-mean polar mean temperatures after minimizing fluctuations of wave-driven dynamical heating.

Figure 11: January-mean NAM index at 50mb vs. years, against total upward E-P flux at 100 mb (normalized by its RMS). The dash-dot line is the trend in NAM index, and the dashed line is the linear regression of F_{100mb}.

Figure 12: January-mean NAM index at 50mb vs. years, against January-mean horizontal E-P flux crossing the box boundary at 50°N (normalized by its RMS). The dash-dot line is the trend in NAM index, and the dashed line is the linear regression of the horizontal E-P flux, with a nearly zero slope.

Figure 13: Angular momentum difference between January-mean and November-mean within the box vs. years, against total upward E-P flux at 100 mb. Both are normalized by their RMS. The dash-dot line is the trend in angular momentum difference, and the dashed line is the linear regression of F_{100mb}.

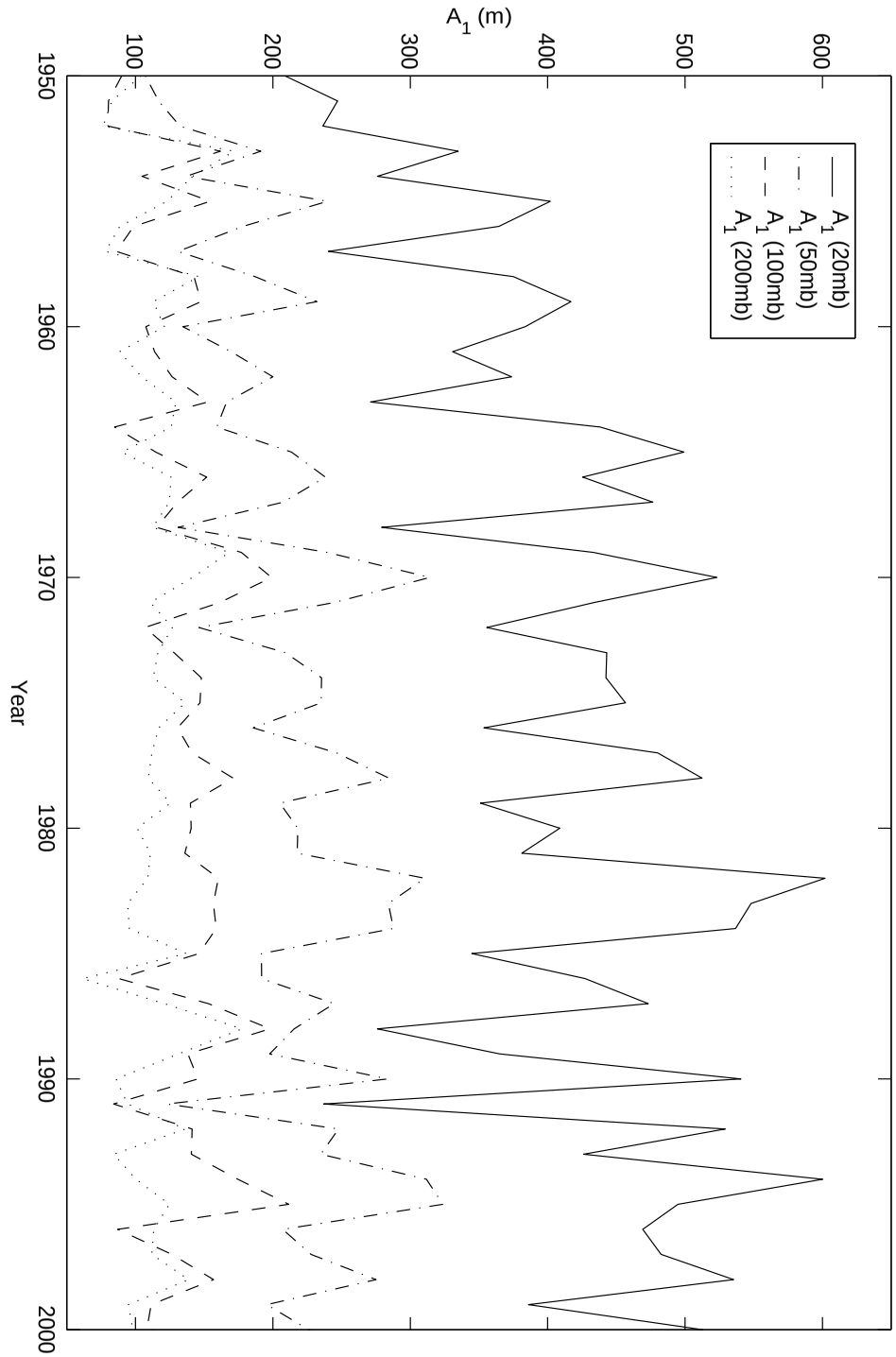
A1 (m)
100
200
300
400
500
600
1950
1960
1970
1980
1990
2000
Year
A1 (20mb)
A1 (50mb)
A1 (100mb)
A1 (200mb)

Figure 1.

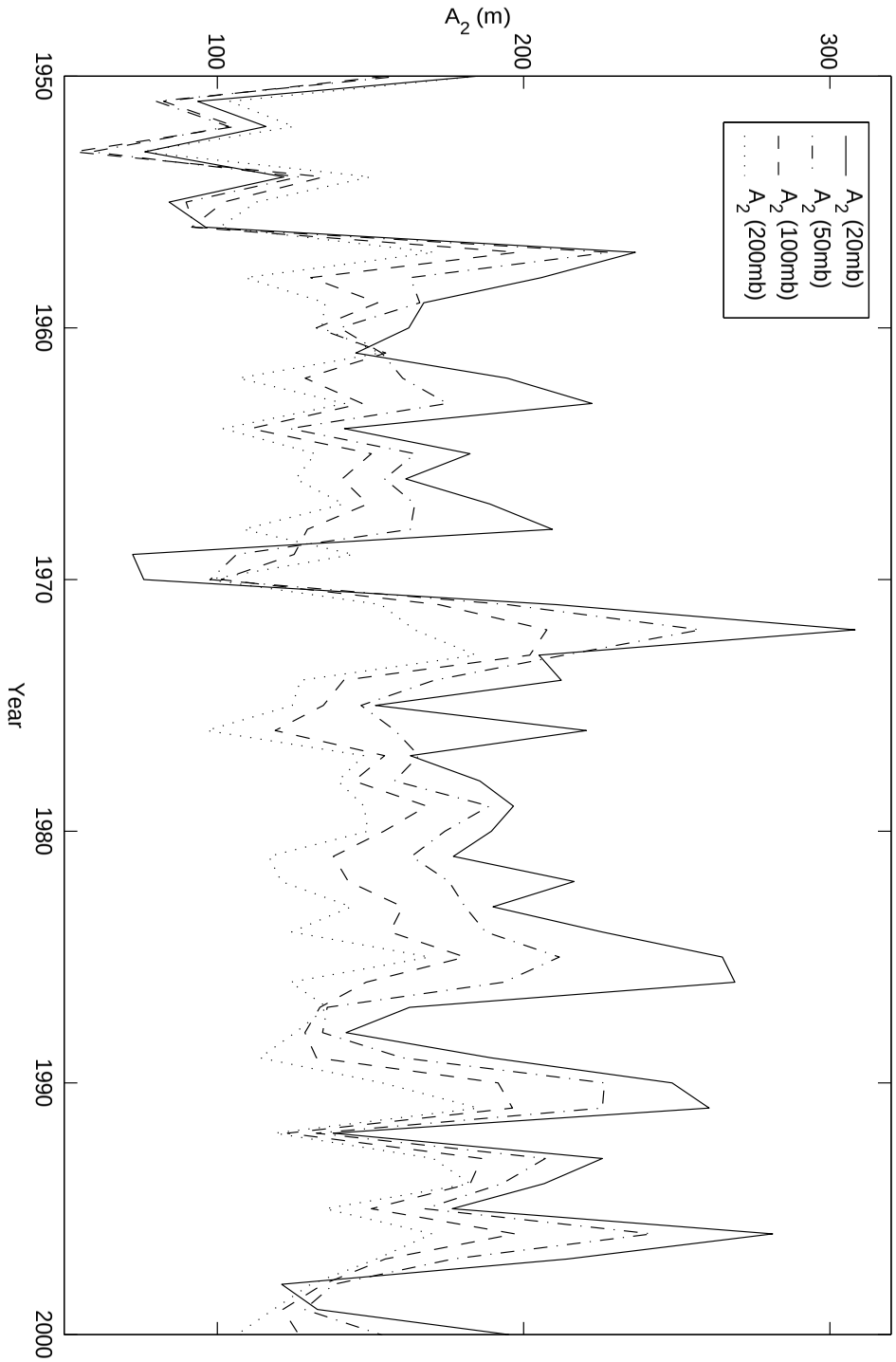
A2 (m)
100
200
300
1950
1960
1970
1980
1990
2000
Year
A2 (20mb)
A2 (50mb)
A2 (100mb)
A2 (200mb)

Figure 2.

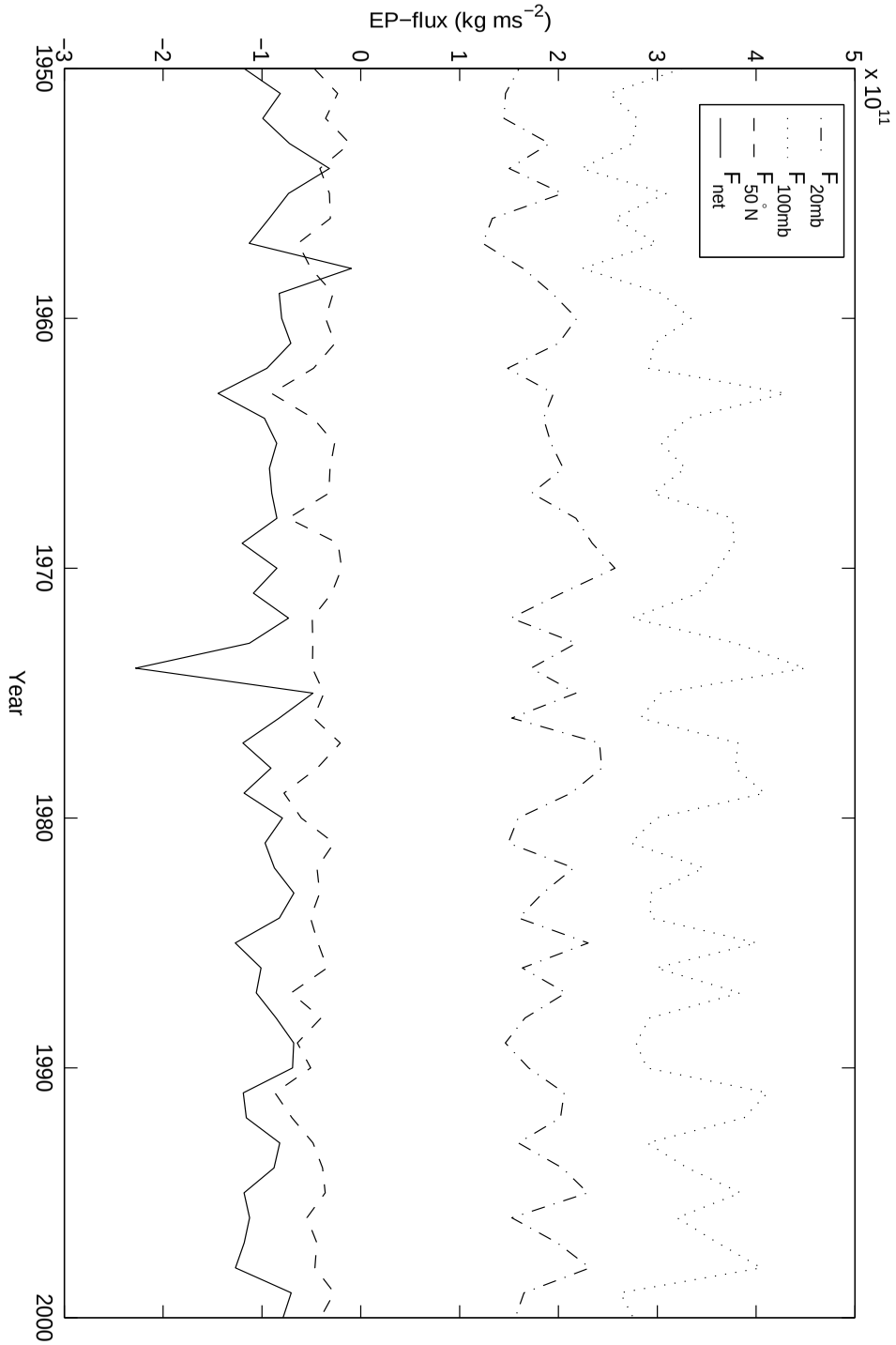
EP−flux (kg ms^{-2})
x 10^{11}
−3
−2
−1
0
1
2
3
4
5
1950
1960
1970
1980
1990
2000
Year
F$_{20mb}$
F$_{100mb}$
F$_{50^\circ N}$
F$_{net}$

Figure 3.

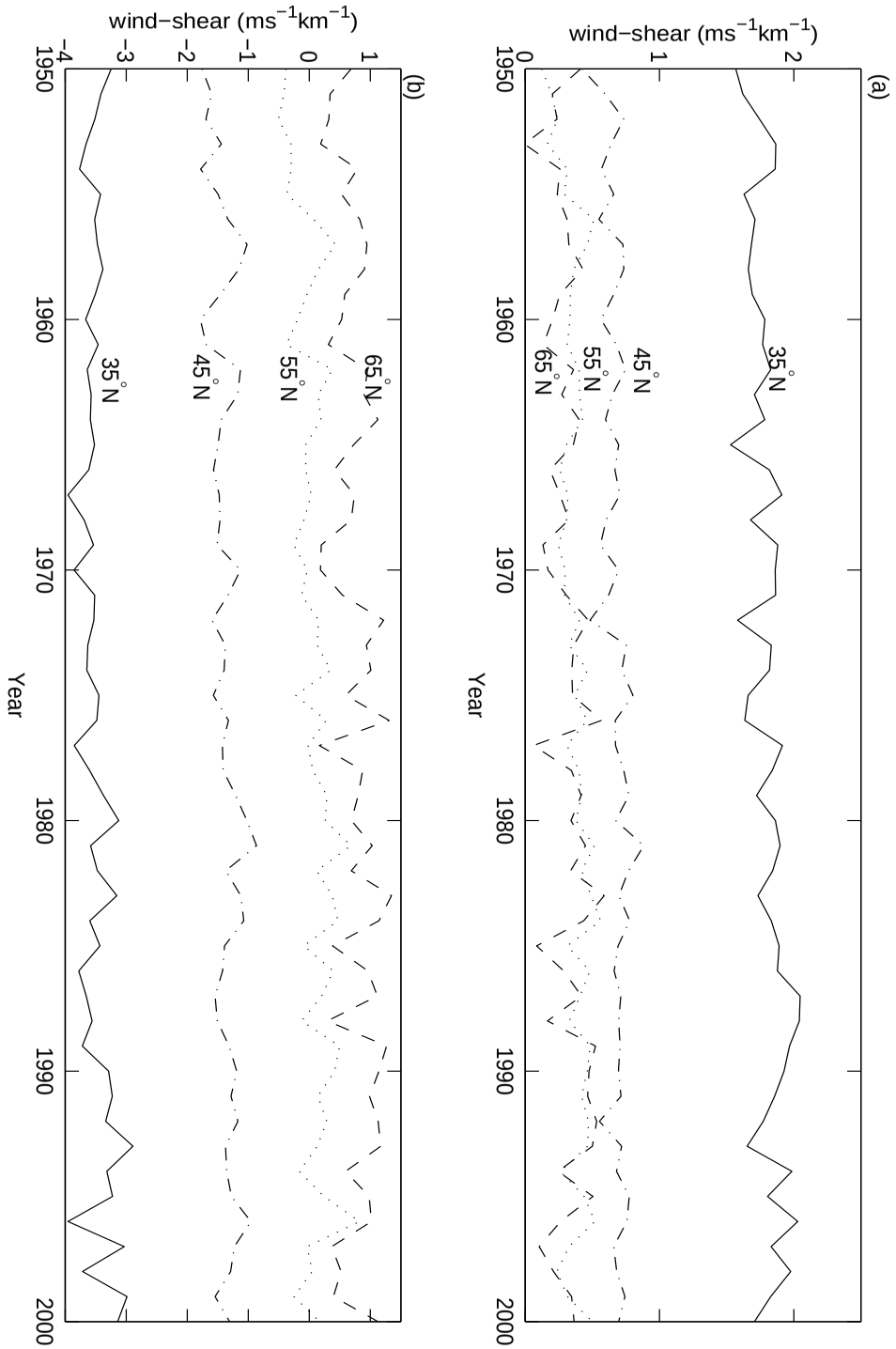
wind−shear (ms^{-1}km^{-1})
(a)
35° N
45° N
55° N
65° N
Year
wind−shear (ms^{-1}km^{-1})
(b)
35° N
45° N
55° N
65° N
Year

Figure 4.

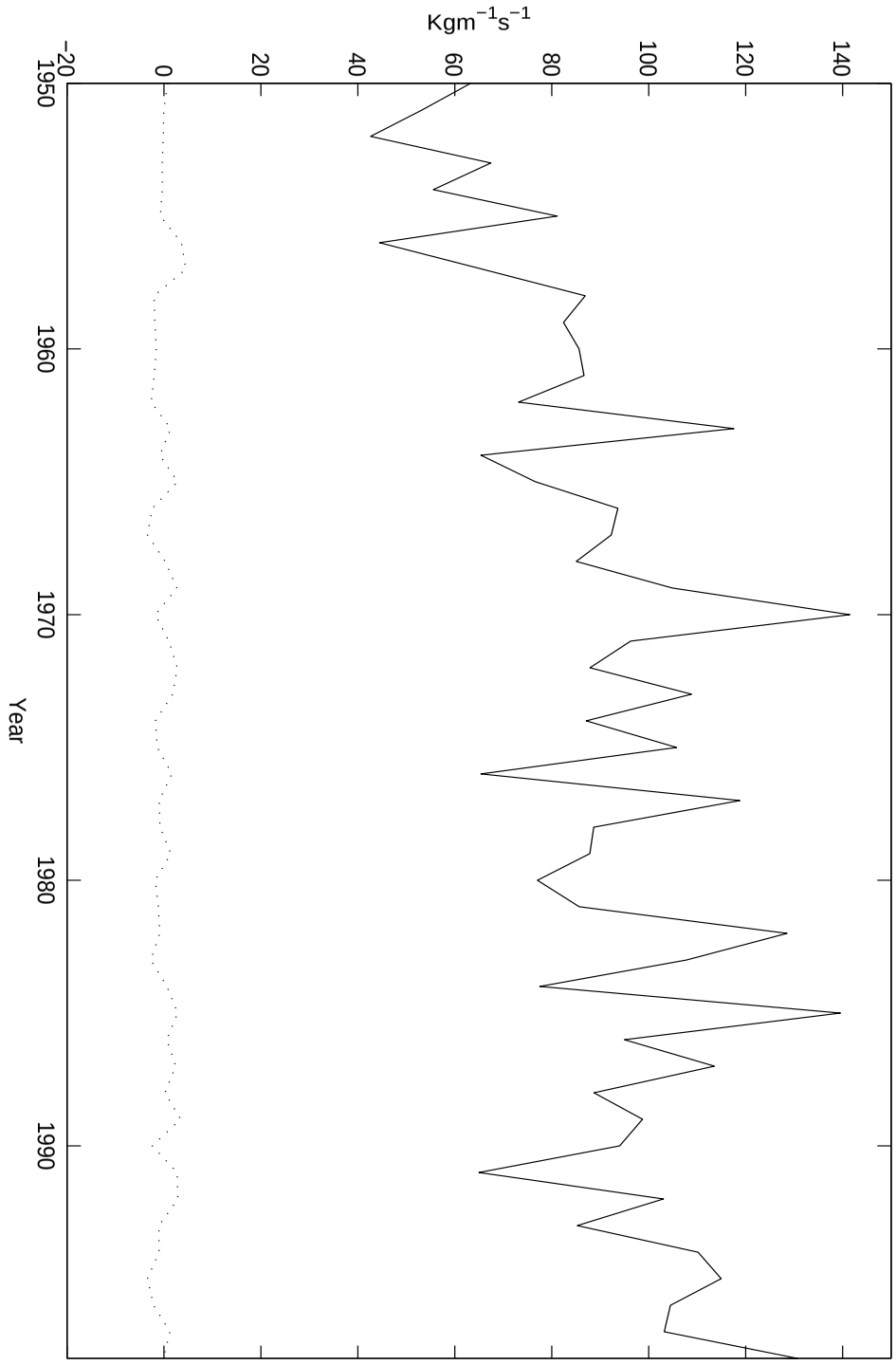
Kgm^{-1}s^{-1}
−20
0
20
40
60
80
100
120
140
1950
1960
1970
1980
1990
Year

Figure 5.

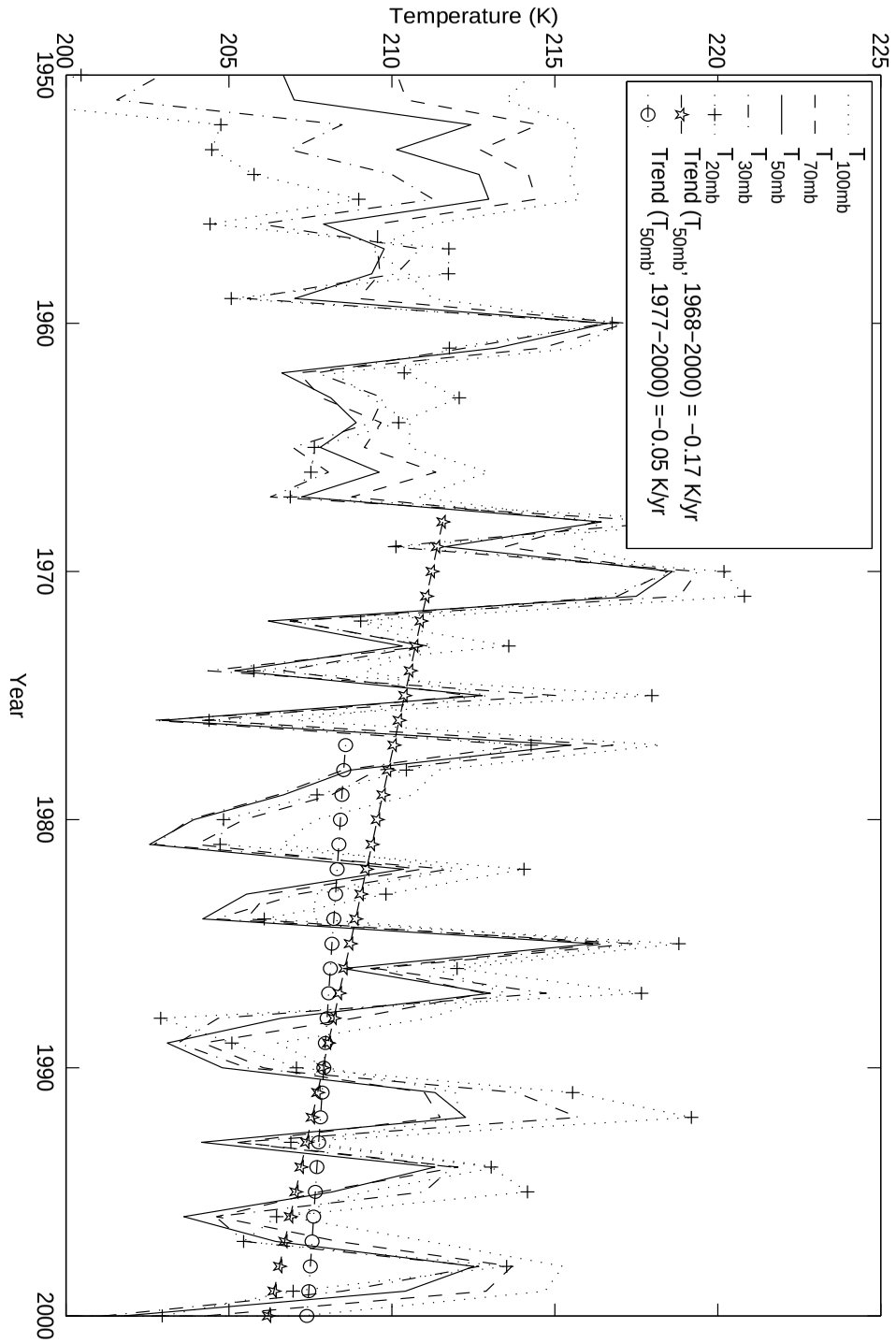
Temperature (K)
200
205
210
215
220
225
1950
1960
1970
1980
1990
2000
Year
T100mb
T70mb
T50mb
T30mb
T20mb
Trend (T50mb, 1968–2000) = −0.17 K/yr
Trend (T50mb, 1977–2000) =−0.05 K/yr

Figure 6.

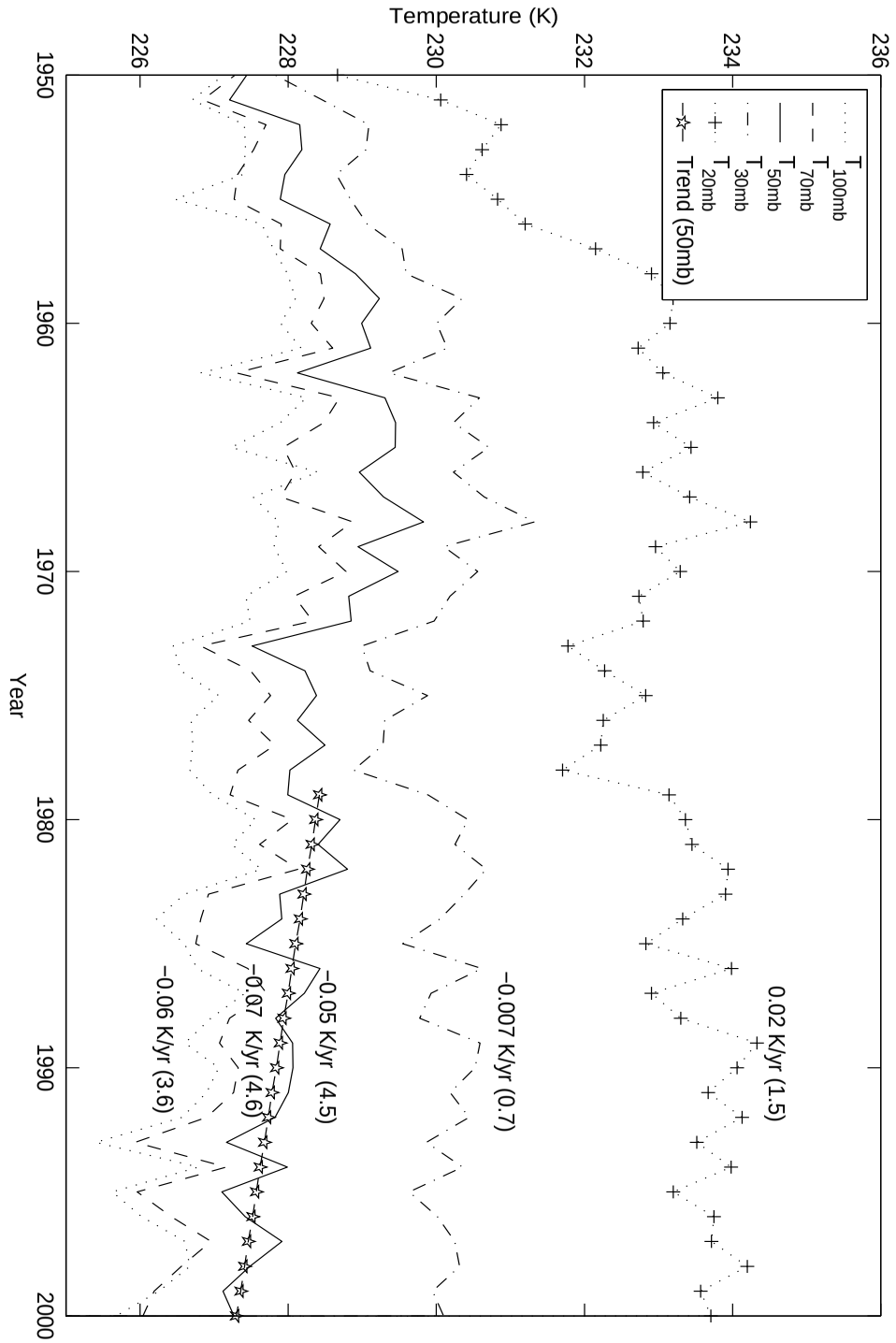
Temperature (K)
226
228
230
232
234
236
1950
1960
1970
1980
1990
2000
Year
T100mb
T70mb
T50mb
T30mb
T20mb
Trend (50mb)
0.02 K/yr (1.5)
−0.007 K/yr (0.7)
−0.05 K/yr (4.5)
−0.07 K/yr (4.6)
−0.06 K/yr (3.6)

Figure 7.

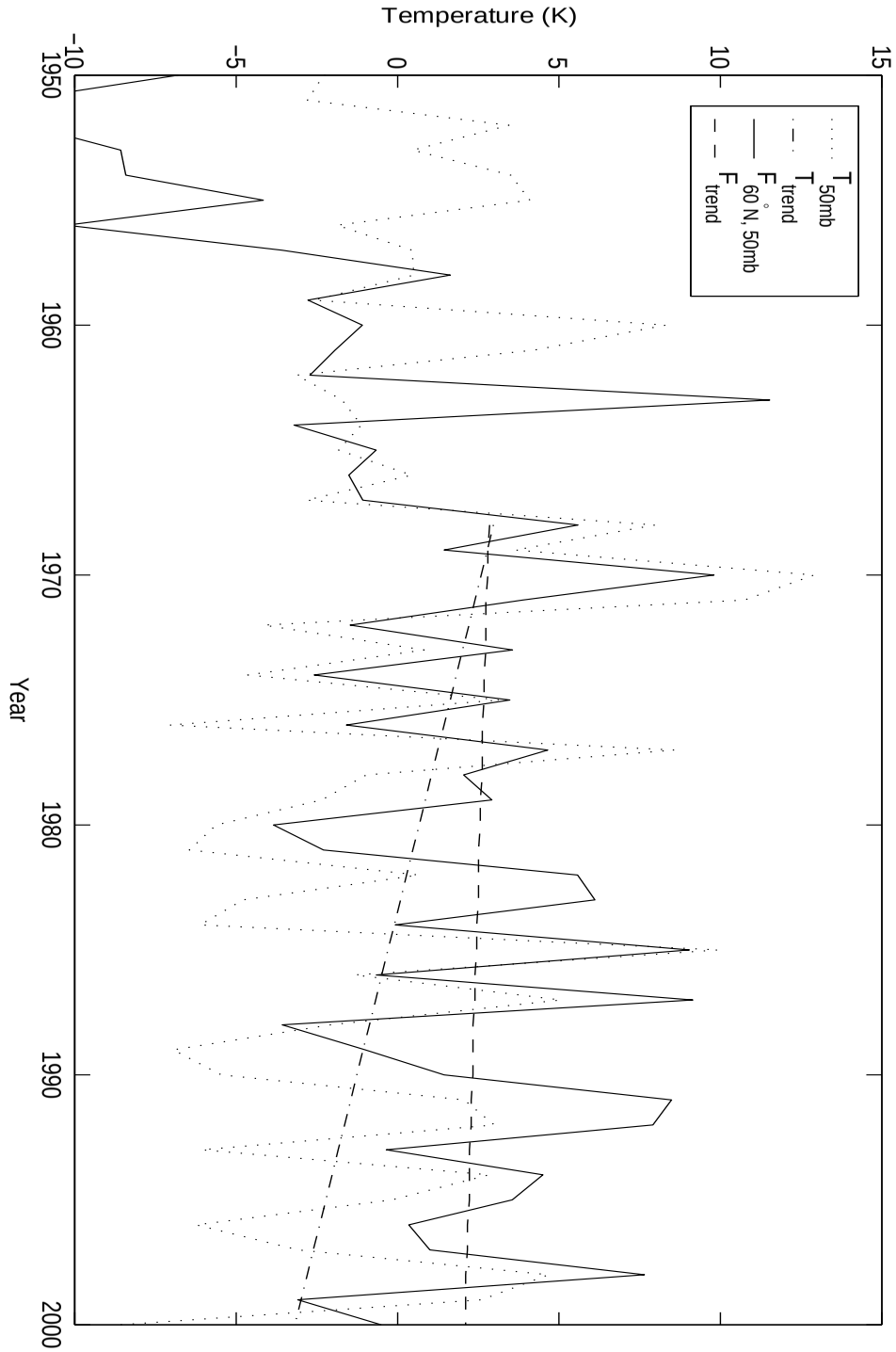
Temperature (K)
−10
−5
0
5
10
15
1950
1960
1970
1980
1990
2000
Year
T 50mb
T trend
F 60°N, 50mb
F trend

Figure 8.

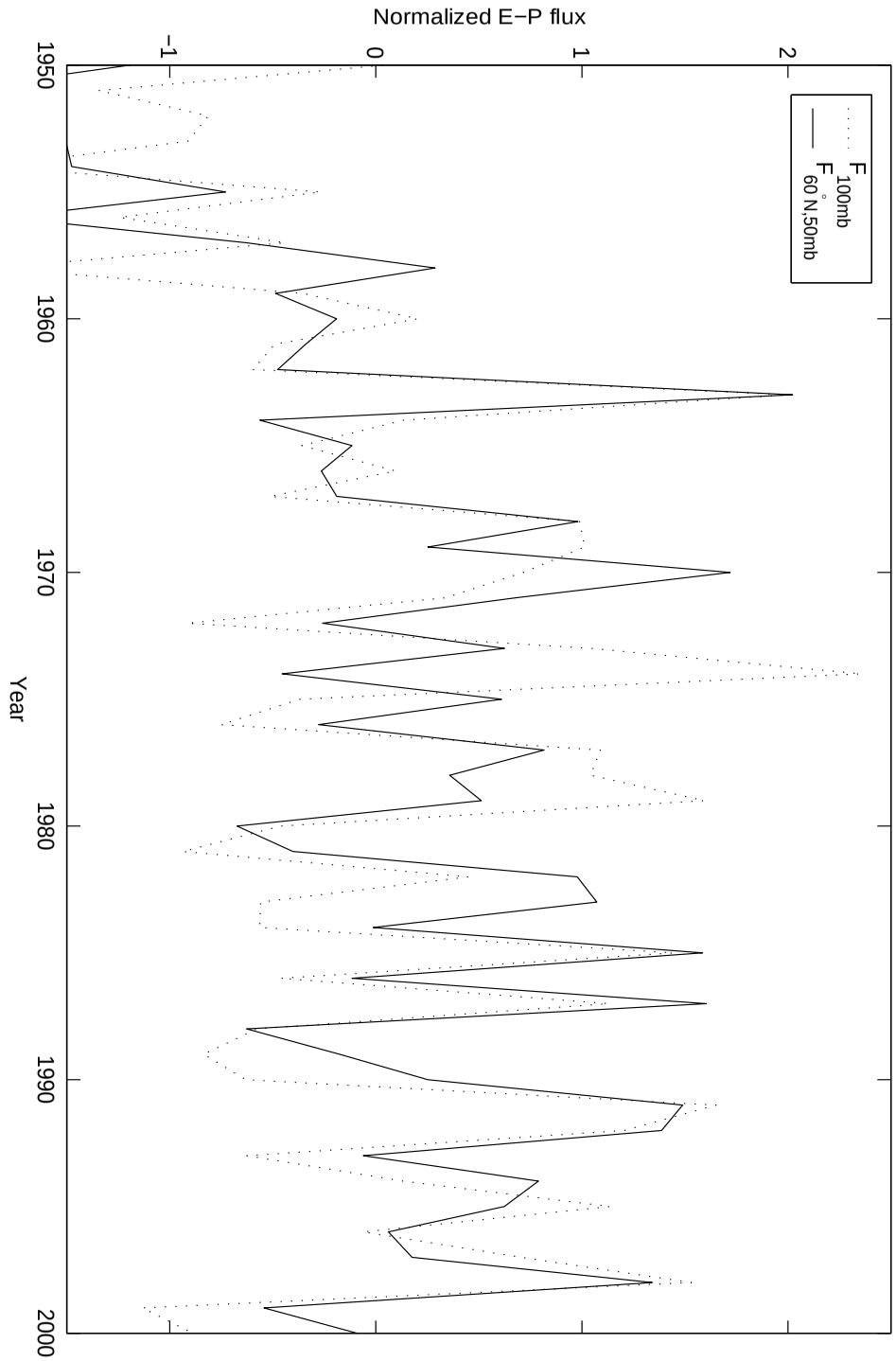
Normalized E−P flux
−1
0
1
2
1950
1960
1970
1980
1990
2000
Year
F 100mb
F 60°N,50mb

Figure 9.

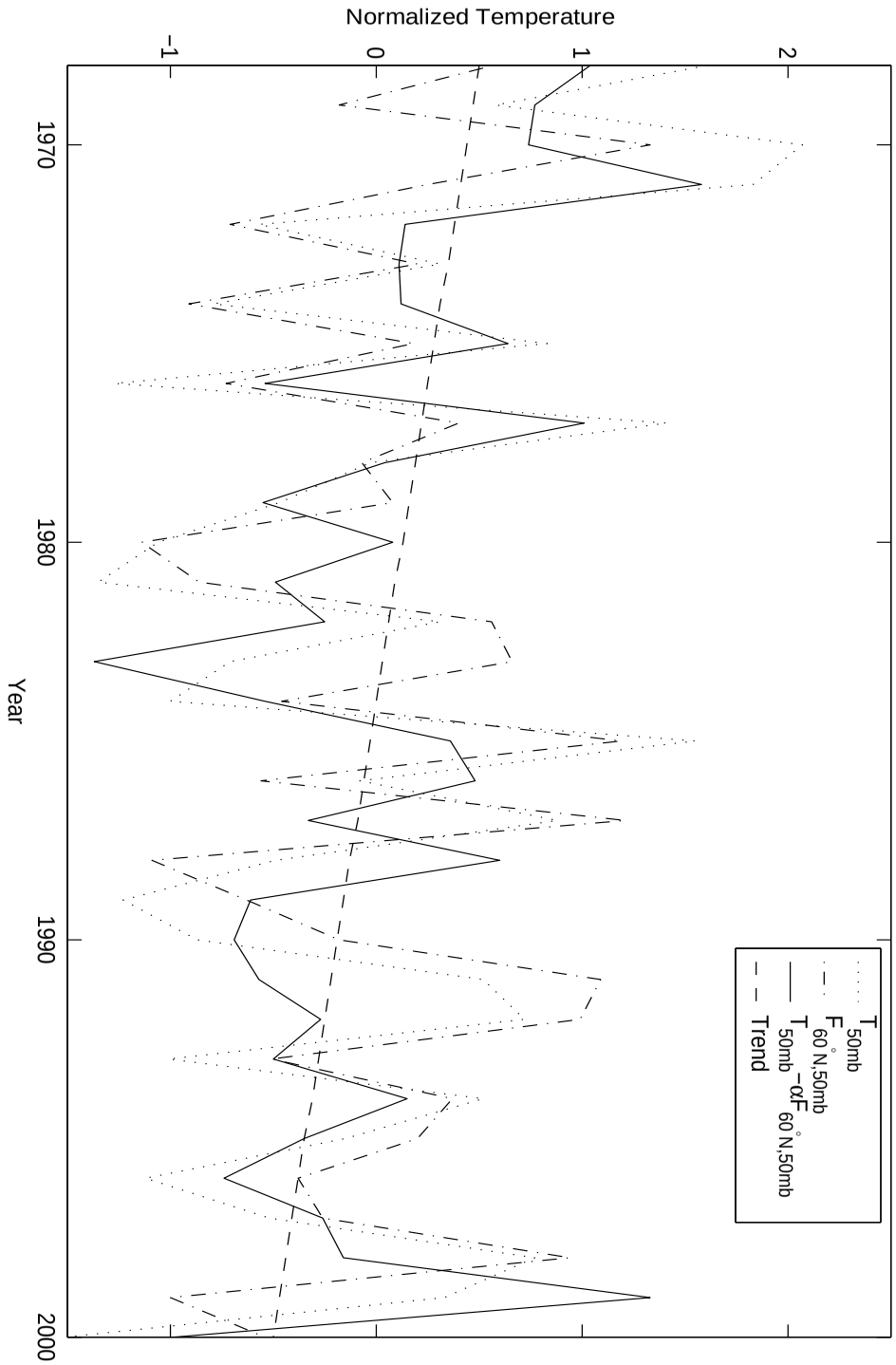
Normalized Temperature
−1
0
1
2
1970
1980
1990
2000
Year
T50mb
F60°N,50mb
T50mb −αF60°N,50mb
Trend

Figure 10.

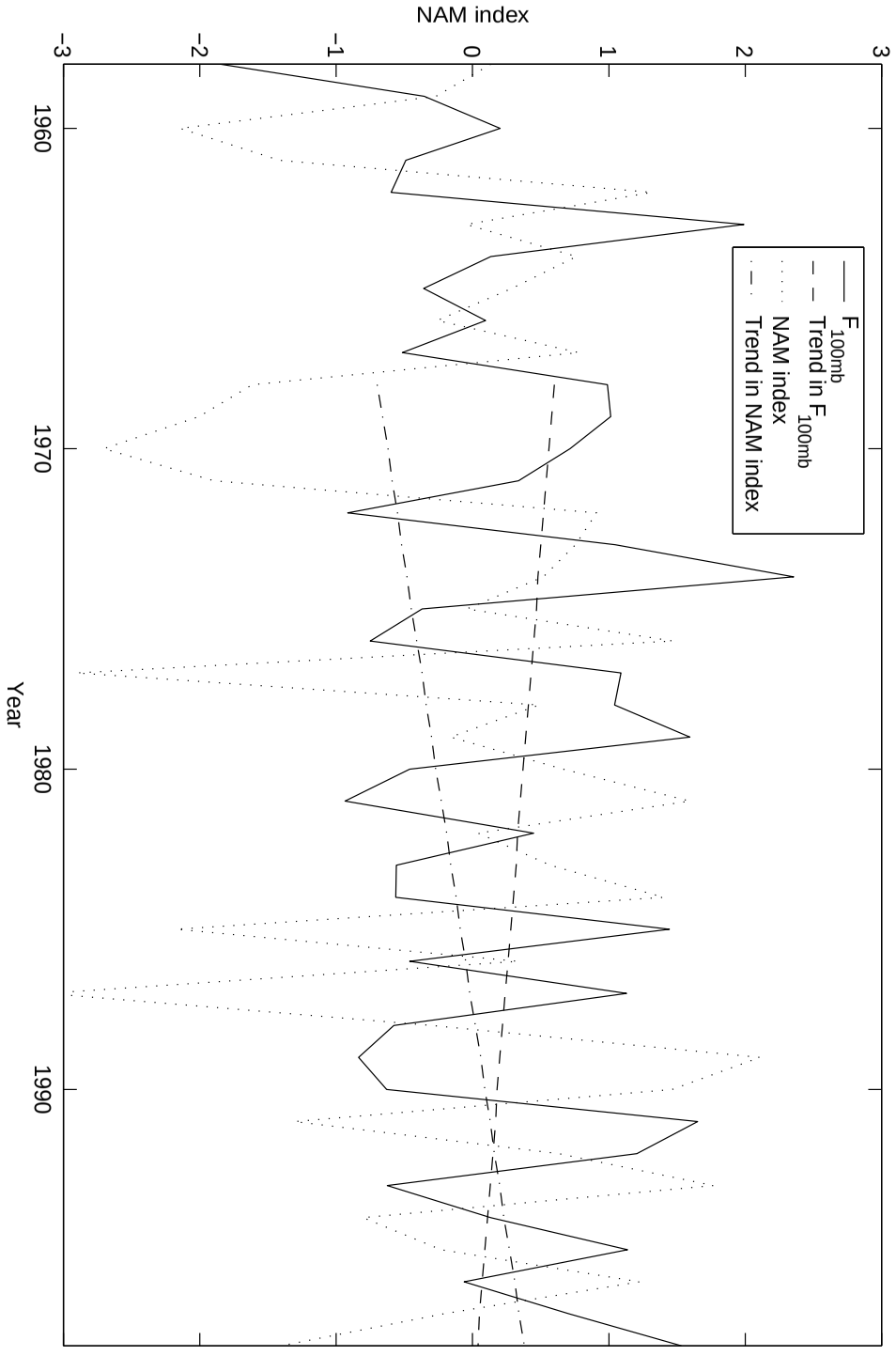
NAM index
−3
−2
−1
0
1
2
3
1960
1970
1980
1990
Year
F100mb
Trend in F100mb
NAM index
Trend in NAM index

Figure 11.

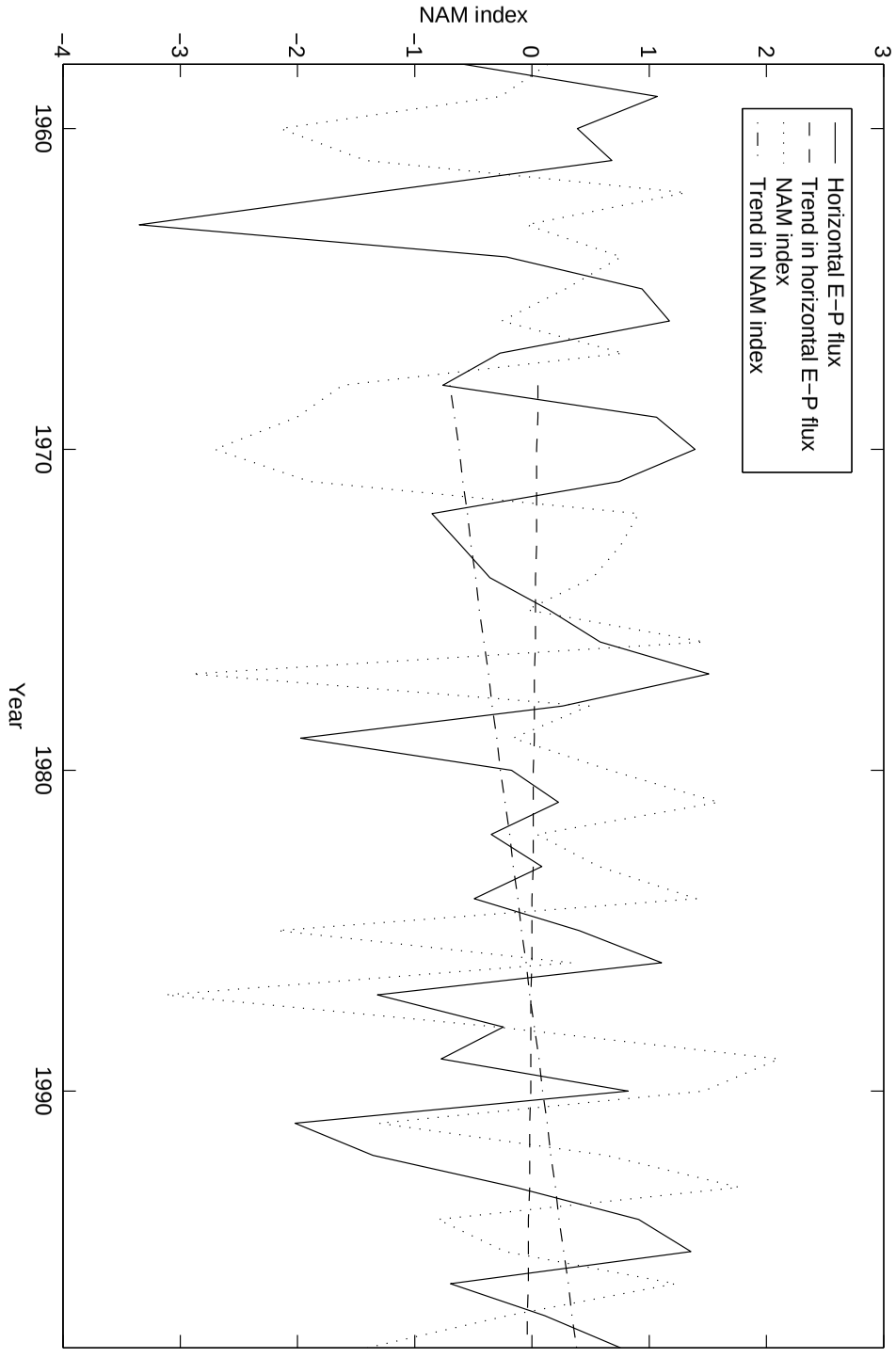
NAM index
−4
−3
−2
−1
0
1
2
3
1960
1970
1980
1990
Year
Horizontal E−P flux
Trend in horizontal E−P flux
NAM index
Trend in NAM index

Figure 12.

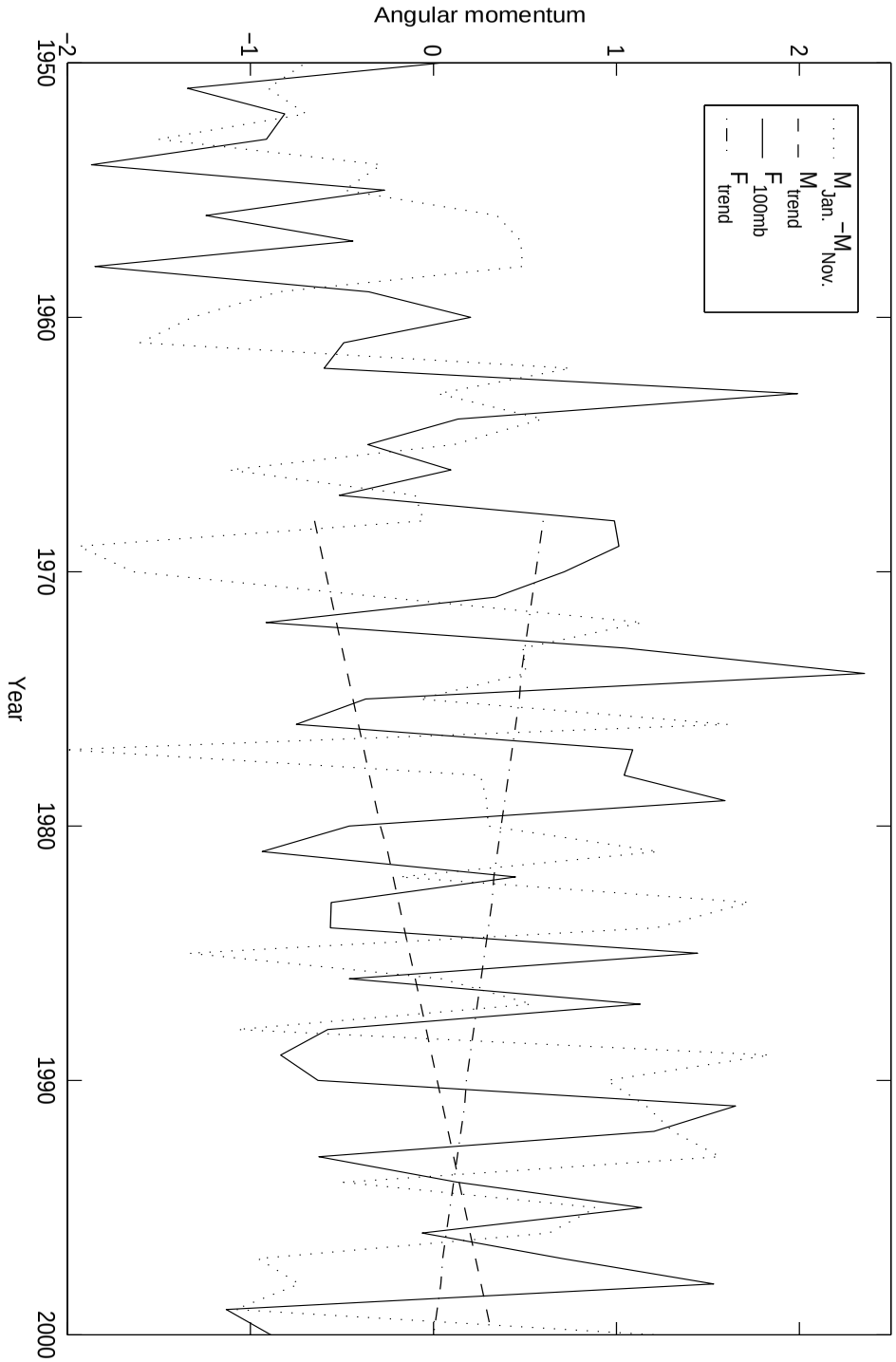
Angular momentum
−2
−1
0
1
2
1950
1960
1970
1980
1990
2000
Year
M Jan. −M Nov.
M trend
F 100mb
F trend

Figure 13.